

## Determining substrate displacement and cell traction fields—a new approach

Zhaochun Yang<sup>a</sup>, Jeen-Shang Lin<sup>b</sup>, Jianxin Chen<sup>a</sup>, James H-C. Wang<sup>a,\*</sup>

<sup>a</sup>*MechanoBiology Laboratory, Departments of Orthopaedic Surgery, Bioengineering and Mechanical Engineering, E1640 Biomedical Science Tower, 210 Lothrop Street, Pittsburgh, PA 15213, USA*

<sup>b</sup>*Department of Civil and Environmental Engineering, University of Pittsburgh, USA*

Received 4 October 2005; received in revised form 4 May 2006; accepted 5 May 2006

Available online 19 May 2006

### Abstract

This paper presents a new approach for the traction force microscopy (TFM) method which determines traction forces exerted by adherent cells on a thin, elastic polyacrylamide gel embedded with fluorescent microbeads. In this enhanced TFM method, a pattern recognition technique is first applied to match the pair of microbead embedded images before and after deformation, which subsequently provides the displacement field of the elastic substrate. Once the displacement field is obtained, the 3-D finite element method (FEM) is used to compute cell traction forces. The new TFM has been applied to determine traction forces of human tendon fibroblasts. Compared to existing TFM methods, the present method has the following advantages: (1) its displacement field obtained is associated with microbead movements; (2) it considers the finite thickness of the thin polyacrylamide gel and is therefore free from the infinite half-space approximation adopted by existing TFM methods; and (3) its computation procedure for determining cell traction forces is fast. © 2006 Elsevier Ltd. All rights reserved.

**Keywords:** Traction; Pattern recognition; Finite element method; Tendon fibroblasts

### 1. Introduction

Cell traction forces play an important role in many biological processes, such as angiogenesis, inflammation, and wound healing (Galbraith and Sheetz, 1998; Kiehart et al., 2000; Lo et al., 2000; Jacinto et al., 2001). A few traction force microscopy (TFM) methods have been developed to determine cell traction forces, such as micromachined substrate (Galbraith and Sheetz, 1997), microneedle-like posts (Tan et al., 2003), micropatterned elastomer (Balaban et al., 2001), and the flat substrate with embedded fluorescent microbeads (Dembo and Wang, 1999; Butler et al., 2002) (Fig. 1). The much stiffer micropatterned elastometer as constructed by Balaban et al. (2001) may also be viewed as a flat substrate as it has a topographic modulation with a height of only 0.3  $\mu\text{m}$ . The flat substrate TFM has a major advantage over the other two methods for its simple boundary conditions and

its applicability in quantitatively determining traction forces of various types of cells such as keratocytes, smooth muscle cells, and fibroblasts (Butler et al., 2002; Beningo et al., 2004; Rajagopalan et al., 2004; Doyle and Lee, 2005; Jurado et al., 2005).

The present approach falls within the flat substrate TFM. We will focus on TFM involving polyacrylamide substrate; however, the force estimation procedure also applies to micropatterned elastometers. This method involves three major steps. The first step fabricates an elastic substrate, which is a thin ( $\sim 70 \mu\text{m}$ ) polyacrylamide gel with embedded fluorescent beads (Beningo and Wang, 2002). The second step computes the bead displacements from a pair of the “null-force” and “force-loaded” images and, thus, defines the displacement field of the elastic substrate. The third step determines cell traction forces from the substrate displacement field based on the theory of elasticity.

Two prominent flat substrate TFM methods, namely DW (Dembo and Wang, 1999) and Butler et al (2002), have been widely used for determining cell traction forces. Both

\*Corresponding author. Tel.: +1 412 648 9102; fax: +1 412 648 8548.  
E-mail address: [wanghc@pitt.edu](mailto:wanghc@pitt.edu) (J.H-C. Wang).

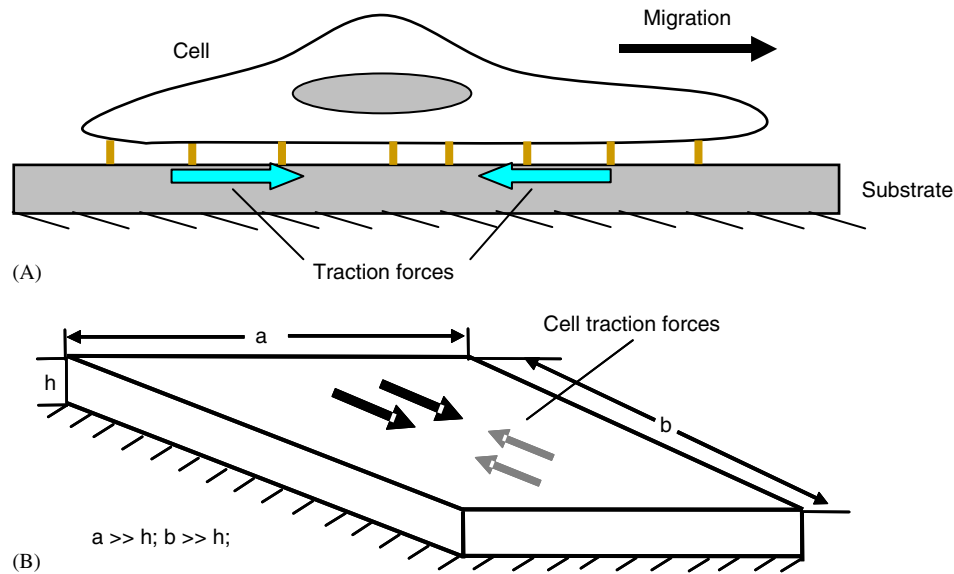


Fig. 1. An illustration of cell traction forces in the flat substrate TFM. (A) A migrating cell that exerts traction forces to underlying substrate; and (B) a thin elastic substrate with cell traction forces. The substrate is in static equilibrium condition.

methods determine first the displacement field from marker displacements and then use them to estimate cell traction forces. In a later paper, Marganski et al. (2003) in which DW are coauthors, they described an “optical flow” algorithm with which the displacement field was obtained through correlation between strain and unstrained images. The DW method formulates the determination of cell traction forces as a regularized inverse problem using Bayesian *a posteriori* statistics. The advantages of the DW method are that it can impose *a priori* error information and model uncertainty in determining the traction force field. It uses displacements from markers that lie inside as well as outside of a cell boundary, and the number of the markers used is larger than the number of forces to be estimated. The regularization scheme guarantees a stable solution but is computationally intensive, as the gradient of the underlying forward model often needs to be re-computed in the search for an optimized answer. In the Butler et al.’s method, the images are first processed for estimating displacement by using small overlapped windows. The windows are typically  $64 \times 64$  pixels on a  $1024 \times 1280$  pixel image. Butler et al (2002) reported the use of distances between successive windows to be 16 pixels. A match is found of one window in the “null-forced” image to that in the “force-loaded” image provided the two windows give the highest cross-correlation. A displacement is defined as the distance between the centers of these two windows. The displacement so estimated is therefore discrete as it is a multiple of the selected distances between successive windows. Moreover, there is an ambiguity as to what the displacement represents.

In computation of traction forces, Butler et al.’s method assumes that forces are applied on a set of periodic grid points, and the displacement at any point can be obtained through a convolution integral. They took the measured

displacement field and carried out the inverse Fourier transform to obtain the force field. This involves a periodicity assumption that the force be distributed over a grid, and that displacements are also computed on a set of grid points. The process is relatively fast; but in general, substituting these forces back would not give the same displacements because of the presence of measurement noises and model errors. Iteration is therefore carried out until the force field obtained gives displacements that are in close match with those estimated for the interior of a cell.

In addition, both the DW and Butler et al. methods are subjected to the same limitation of assuming the thin polyacrylamide substrate to be an infinite half-space in order to apply the Boussinesq analytical solution (Landau and Lifshitz, 1986). It has been noted that the assumption of the infinite half-space is only valid when the lateral dimensions of the cell and the lateral distances over which displacements are measured are both small compared with the gel thickness (Butler et al., 2002). But this may not always be the case. Often the cell dimension is close to the thickness of a typical polyacrylamide gel substrate. This is particularly so in the case of fibroblasts, whose lengths are typically in the neighborhood of  $50 \mu\text{m}$ , as compared to the gel substrate thickness of about  $70 \mu\text{m}$ .

To get a sense of how the half-space approximation fares in modeling thin gel substrates, we have conducted analyses using 3-D finite element method (FEM). We employed three square substrates, with each having the same surface area of  $1000 \times 1000 \mu\text{m}^2$ , but was given a different thickness. The three substrate thicknesses used were 1000, 200 and  $70 \mu\text{m}$ , respectively. Each substrate was fixed at the bottom surface and was subjected to a point surface load of 10 nN at the center of the top surface. The resulting displacements are summarized in Fig. 2A. It clearly shows that substrate thickness does affect the

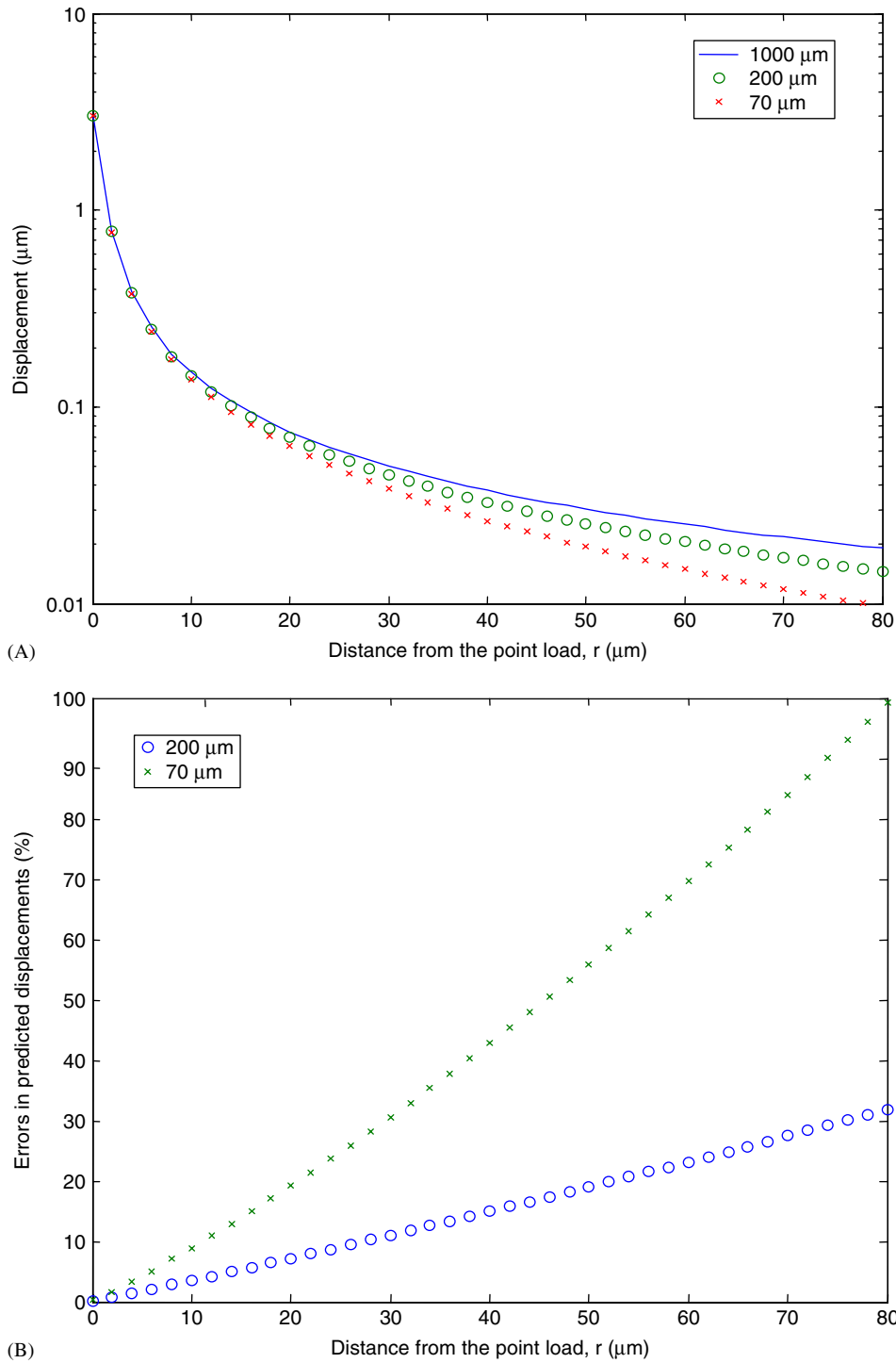


Fig. 2. Effects of substrate thickness on displacements due to a point surface load. (A) The displacement responses due to a point load; and (B) the errors in displacement estimates by assuming the substrates to be very thick (1000 μm).

magnitudes of the induced displacements. As expected, the displacements obtained for the substrate with 1000 μm agree well with the Boussinesq solution, with differences less than 5% if singularity of the latter is excluded. This, conversely, also means that the half-space approximation does not work that well for the other two thinner substrates. The differences in the displacements may not

be large, but the ratio can be substantial. Fig. 2B shows the errors one may incur in projecting the displacements for these two thinner substrates using the semi-half space approximation. Whether or not this constitutes a problem depends upon the problem at hand. For the objectives of estimating cell forces from displacement measurements, implications derived from Fig. 2B could potentially affect

the way one uses Boussinesq solution in obtaining traction force from displacement and this requires further investigation.

To alleviate the aforementioned limitations of the existing methods, we have developed an alternative flat substrate TFM method. Herein we present the new approach, which is followed by a description of its application to determine traction forces of human tendon fibroblasts.

## 2. Methods

The present method in determining cell traction forces (Fig. 3) is described in this section. It involves three steps: (1) locating the beads in the images of the polyacrylamide substrate; (2) matching beads from the “null-force” image to those of the “force-loaded” image and deriving the displacement field; and (3) computing cell traction forces using the 3-D FEM.

### 2.1. Locating the beads in images

“Null-force” and “force-loaded” images are the images of the fluorescent bead-embedded gel substrate that are taken before and after deformation caused by cell traction forces. Each pixel in the image has a gray value defined as an 8-bit unsigned integer. Beads are fluorescent and their gray values are higher than those of the background. This brightness contrast is the basis for locating beads of this study. However, the brightness of the background varies throughout an image, and it is not feasible to define a global threshold of the gray value for distinguishing beads from background. A localized identification approach was devised, as described next.

We divided each image into  $6 \times 6$  pixel squares and computed the mean of the gray values in each square as a local threshold. The 8-bit gray value of each pixel was converted to a binary value of 0 for black or 1 for white, depending on whether or not its gray value lay below or

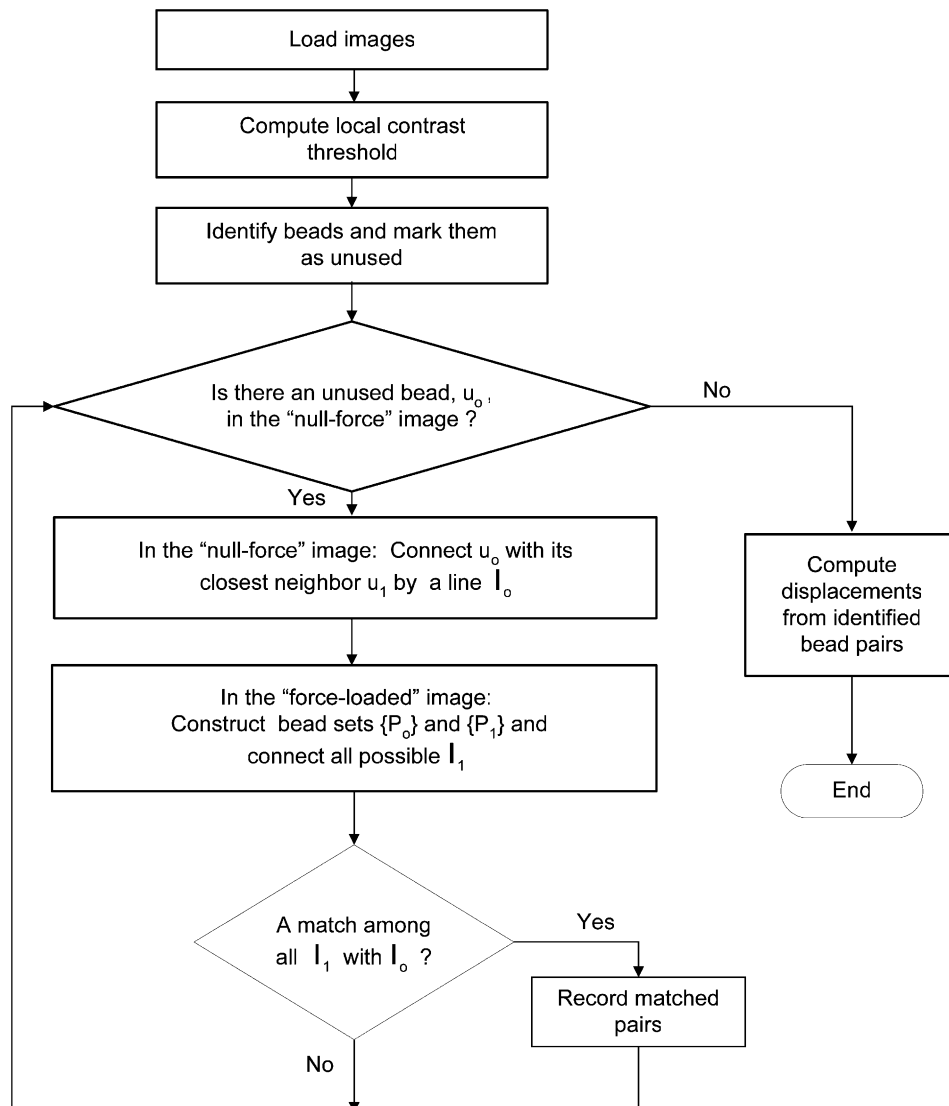


Fig. 3. A flow chart illustrating the procedures used in the new TFM method in determining the displacement field of the substrate.

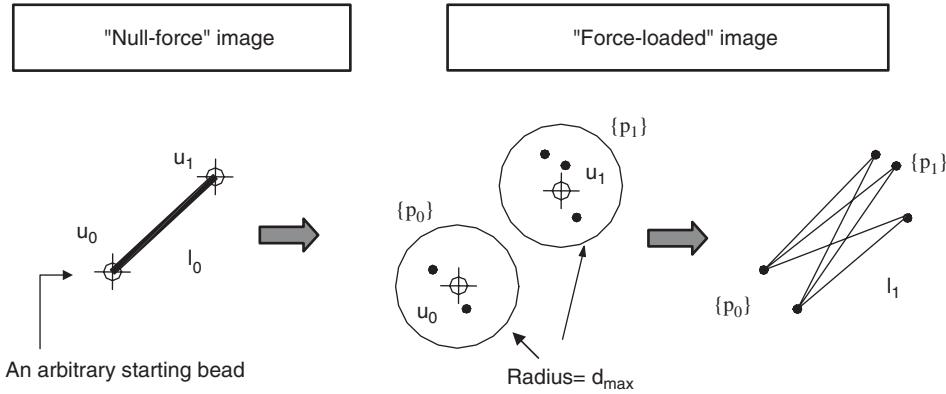


Fig. 4. A schematic view of the bead matching algorithm.

above the threshold. Each connected 1 cluster is called a spot. A spot is deemed a likely bead if its size is compatible to that of a bead image. The bead size used for this study was  $0.2\mu\text{m}$  in diameter, and the magnification scale was  $0.233\mu\text{m}/\text{pixel}$ . As such, a bead would have occupied about 1 pixel on the image. Because of light spread, a bead would appear at least as 4 pixels in size, but with a higher brightness at the center. In this study, spots that have a size greater or equal to 4 and smaller or equal to 8 pixels are treated as beads. Spots greater than 8 pixels may represent a group of beads that were close. They were not used to avoid poor resolution as the center of the spot may significantly deviate from any of the beads in the group. On the other hand, spots smaller than 4 were not used to reduce the chances of matching errors. Using a different selection criterion, one may get a different number of beads; this is not critical, however. What is critical is that we need the spots identified to be distributed randomly so that later on we can estimate the displacement field throughout an image. Once a spot is accepted, its mass center is registered as the center of a bead.

### 2.2. Pattern recognition in identifying pairs of beads

After locating all spots or beads in the “null-force” and “force-loaded” images, the next step is to pair them. We devised a pattern recognition technique as follows. First, we defined the upper bound displacement of the substrate,  $d_{\text{max}}$ , as twice the maximum expected displacement. In the experiment described in this study, the maximum displacement was expected to be about  $1\mu\text{m}$ , and we used  $2\mu\text{m}$  as an estimate for  $d_{\text{max}}$ . Second, we started with an arbitrary bead on the “null-force” image,  $\mathbf{u}_0$ , and found its closest neighbor,  $\mathbf{u}_1$ , and connected them with a line segment denoted as  $l_0$ . Third, we found two bead sets  $\{\mathbf{P}_0\}$  and  $\{\mathbf{P}_1\}$  on the “force-loaded” image such that

$$\{\mathbf{P}_0\} = \{\mathbf{p} \mid |\mathbf{p} - \mathbf{u}_0| \leq d_{\text{max}}, \mathbf{p} \in \text{force-loaded image}\}, \quad (1)$$

$$\{\mathbf{P}_1\} = \{\mathbf{p} \mid |\mathbf{p} - \mathbf{u}_1| \leq d_{\text{max}}, \mathbf{p} \in \text{force-loaded image}\}, \quad (2)$$

Fourth, we connected all possible pairs of beads from  $\{\mathbf{P}_0\}$  to  $\{\mathbf{P}_1\}$  and denoted each as an  $l_1$ . This is depicted in

Fig. 4. Fifth, we determined if there was a match between  $l_0$  and  $l_1$ . At the end of matching, bead  $\mathbf{u}_0$  is marked as used even if no match is found. If a match is found, we recorded the coordinates of both  $\mathbf{u}_0$ ,  $\mathbf{u}_1$  and their counter parts. A new search is repeated using  $\mathbf{u}_1$  as the new originating point for constructing  $l_0$ . This process continues until all beads in the “null-force” image have been marked as used.

### 2.3. Line matching criteria

We developed the matching criteria based upon the levels of expected strains. Basically, two lines can only be a match if their lengths are compatible with the expected normal strain, and their angular shift is below the expected shear strain. This is approximately translated into the following criterion:

$$\kappa = \frac{\max(|l_0|, |l_1|)}{\min(|l_0|, |l_1|)} \leq 1 + c_1 \varepsilon_{\text{max}}, \quad (3)$$

$$\chi = |\alpha_0 - \alpha_1| \leq c_2 \gamma_{\text{max}}, \quad (4)$$

where  $|l_0|$  is the length, and  $\alpha_0$  is the angle of the line segment  $l_0$ , whereas  $|l_1|$  and  $\alpha_1$  are their counter parts for  $l_1$ . Also,  $\varepsilon_{\text{max}}$  is the estimated maximum normal strain,  $\gamma_{\text{max}}$  the maximum shear strain,  $C_1$  and  $C_2$  are amplification factors that lie between 1 and 2. The angles are measured from the positive horizontal direction in a counterclockwise manner.

Apparently, application of these criteria requires judgments. In this study we have found that the use of  $c_1 \varepsilon_{\text{max}} = 0.2$  and  $c_2 \gamma_{\text{max}} = 10^\circ$  to give satisfactory results. When more than one  $l_1$  matches, we chose the one with the minimum normalized deviation,  $\zeta$ , as follows:

$$\zeta = \sqrt{\left(\frac{\kappa}{1 + c_1 \varepsilon_{\text{max}}}\right)^2 + \left(\frac{\chi}{c_2 \gamma_{\text{max}}}\right)^2}. \quad (5)$$

### 2.4. Determining the displacement between pairs of beads

Only bead pairs that are matched between two images are kept. The  $x$ - and  $y$ -displacement of any bead from the “null-force” image is simply a difference in the coordinates

as follows:

$$dx_0 = x - x_0,$$

$$dy_0 = y - x_0 \quad (6)$$

where  $dx_0, dy_0$  are the displacements of bead  $o$  in the “null-force” image that has moved from  $(x_0, y_0)$  to  $(x, y)$ .

As the beads identified generally are scattered rather randomly over an image, a linear interpolation of the displacement field was carried out to provide displacement on the FE nodes. In this study, we used a regular lattice in constructing a 3-D finite element mesh model of the substrate. The lattice has a dimension of  $4.66 \mu\text{m} \times 4.66 \mu\text{m} \times 14 \mu\text{m}$  in  $x, y$  and  $z$  directions, respectively. In other words, each element covers a  $20 \times 20$  pixels area of the image.

The displacement field obtained may contain rigid body motion due to measurement noises and identification errors. For the problem studied, at locations about  $20 \mu\text{m}$  away from the cell boundary, the displacements are negligible. A linear trend in the displacement from the far field data thus gives the rigid body translation and rotation. This is obtained via linear least square fit. The rigid body motion is subtracted from the displacement of each node before further processing.

### 2.5. Computing cell traction forces

Once the substrate displacement field is defined, 3-D FEM is applied to determine cell traction forces. In our FEM model, the thin gel substrate is represented as a plate of finite size. Eight-node isoparametric brick finite elements were used in this study.

Since the elastic substrate is in equilibrium condition, the following static equilibrium equation must hold:

$$[K]\{u\} = \{F\}, \quad (7)$$

where  $[K]$  is the global stiffness matrix,  $\{u\}$  the nodal displacement vector, and  $\{F\}$  the nodal force vector.

The equilibrium condition can further be written in terms of sub-matrices and sub-vectors as

$$\begin{Bmatrix} [K_{cc}] & [K_{cs}] \\ [K_{cs}]^T & [K_{ss}] \end{Bmatrix} \begin{Bmatrix} \{u_c\} \\ \{u_s\} \end{Bmatrix} = \begin{Bmatrix} \{F_c\} \\ \{F_s\} \end{Bmatrix}, \quad (8)$$

where  $s$  subscript denotes the degrees-of-freedom (DOFs) where displacements are known; and  $c$  subscript denotes the rest of the DOFs where the forces are known.

For nodes outside the areas that are in contact with the cell, their nodal forces are zero. By incorporating this information, the above equation becomes

$$\begin{Bmatrix} [K_{cc}] & [K_{cs}] \\ [K_{cs}]^T & [K_{ss}] \end{Bmatrix} \begin{Bmatrix} \{u_c\} \\ \{u_s\} \end{Bmatrix} = \begin{Bmatrix} \{0\} \\ \{F_s\} \end{Bmatrix}. \quad (9)$$

Similar to Butler et al.’s constrained approach, we do not use marker displacements from the exterior of a cell. As

they pointed out that the displacement falls off from a particular traction point rather fast and the information content of displacements exterior to a cell is rather low (Butler et al., 2002). Furthermore, the first row of the above equation enables the expression of displacements for all traction-free points  $\{u_c\}$  in terms of known displacement  $\{u_s\}$  as

$$\{u_c\} = [K_{cc}]^{-1}(-[K_{cs}])\{u_s\}. \quad (10)$$

Therefore, after substitution, the force vector corresponding to the imposed displacement vector  $\{u_s\}$  can be found as follows,

$$\{F_s\} = (-[K_{cs}]^T[K_{cc}]^{-1}[K_{cs}] + [K_{ss}])\{u_s\}. \quad (11)$$

Eq. (11) is the key equation that gives the traction forces exerted by the cells. With these forces known, the traction stresses on the top of the substrate can be determined. The only inversion of the present formulation involves the inverse of  $[K_{cc}]$  matrix. As the matrix is positive definite, its inverse always exists. Eq. (11) is used to compute cell traction forces of the present study.

The required input to the 3-D FEM analysis includes the Young’s modulus and the Poisson’s ratio of the substrate, the fixed boundary conditions at the bottom of the substrate, and the nodal numbers where the forces are zero, as well as the displacement field inside the cell. We used a general-purpose FEM code (ANSYS 8.0) to obtain the cell traction forces.

### 2.6. Evaluation of the present method through simulation

We conducted numerical simulation tests to evaluate the present method. As we deal with only elastic substrate, Eq. (11) is linear and that any variation, such as a noise in  $\{u_s\}$ , causes a proportional change in the resulting traction forces. In other words, the effects of measurement noises are known. This leads us to focus the investigation on whether or not we can recover the known displacements of the beads in the absence of noise.

We numerically created a pair of the “null force” and the “force-loaded” images in the following fashion. First, a “null force” image of  $300 \times 300$  pixels, as depicted in Fig. 5A, was generated using a magnification scale of  $0.233 \mu\text{m}/\text{pixel}$ . Each bead had a diameter of  $0.5 \mu\text{m}$ . Beads were first distributed using a grid pattern with a grid spacing of 30 pixels, followed by a random shift in both the  $x$ - and  $y$ -directions using a uniform distribution with an amplitude between 0 and 10 pixels. In our study, we found the gray values of an image generally lie within a narrow range, with the maximum contrast equals to about 45. To be compatible with the laboratory obtained images, we used in the simulation gray values between 175 and 219. The former was adopted for the background, the latter as the center of a bead. Within each bead the gray value was modeled to increase linearly from the background at the edge of a radius to the maximum value at the center of a bead.

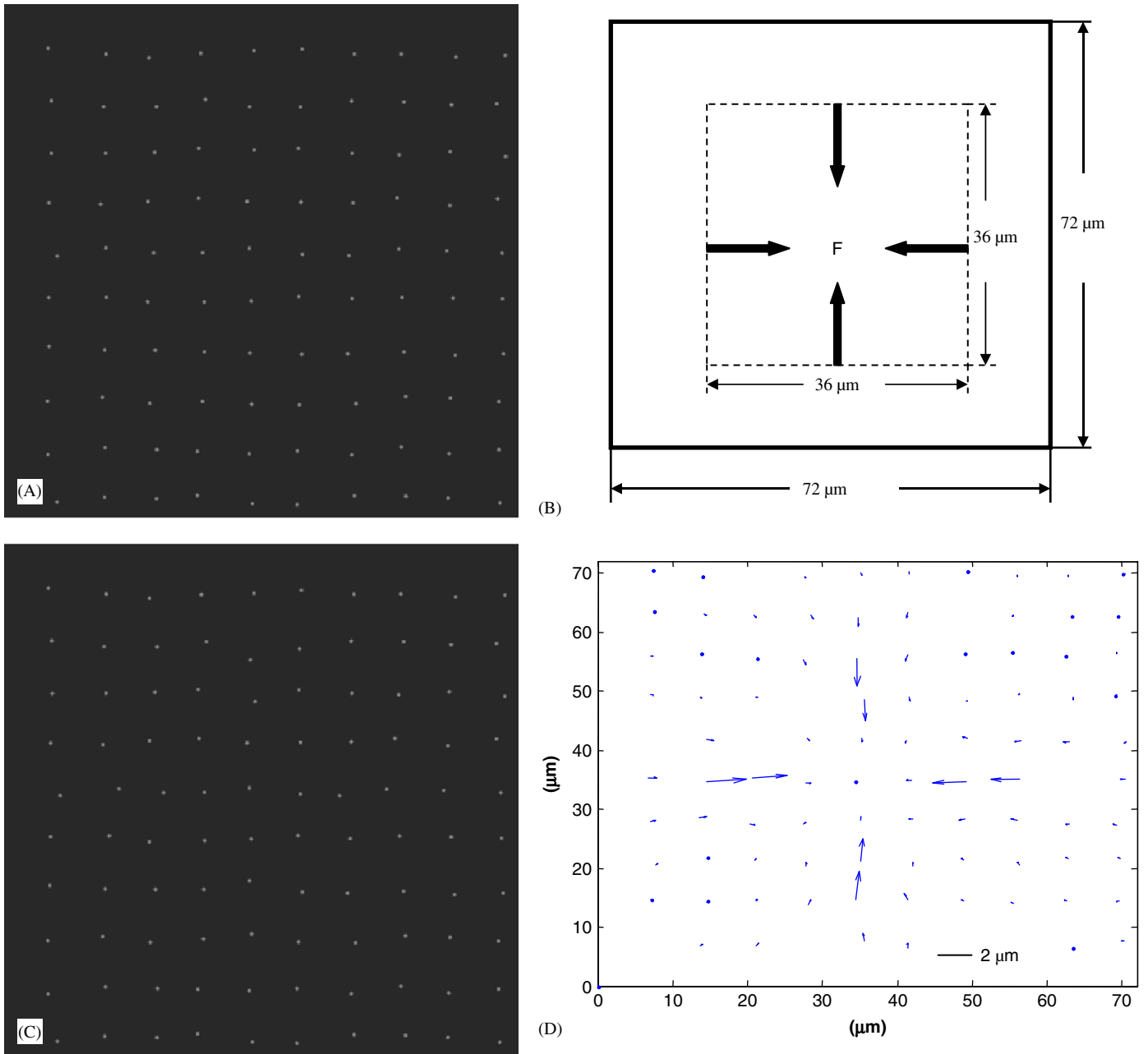


Fig. 5. A simulation test to validate algorithms for determining substrate displacement field. (A) A simulated “null-force” image; (B) two pairs of balanced forces used in generating displacement field for the study; (C) the generated “force-loaded” image; and (D) the recovered displacement field.

Second, a displacement field was created by applying two pairs of balanced forces on the surface of an elastic substrate, as illustrated in Fig. 5B, to simulate cell traction. Each of the force had a magnitude of 8 nN. The displacement field was computed using a Young’s modulus of 3 kPa and a Poisson ratio of 0.4 for the substrate. The resulting displacement field is summarized in Fig. 5B. Third, this displacement field was then imposed on each bead to obtain the “force-loaded” image of Fig. 5C. Fig. 5A and C formed the base image pair for the recovery of the displacement field. The recovered displacement field is summarized in Fig. 5D. The mean  $\pm$  standard deviations

of the errors for the  $x$ - and  $y$ -displacements were found to be  $0.033 \pm 0.023$  and  $0.033 \pm 0.024$   $\mu\text{m}$ , respectively, with the corresponding maximum errors of 0.088 and 0.098  $\mu\text{m}$ , respectively. This maximum error amounts to about 0.42 pixels on the image. It is interesting to note that this error was obtained without introduction of noise into the simulation. As it turned out this error is intrinsic to the process and it is not possible to reduce it. Specifically, the error can be attributed to the inability to locate bead center exactly. This occurs whenever the center of a bead does not lie on a pixel of an image, or that the identified bead pixels are not symmetric about the bead center. Even

if a bead center was originally placed exactly on a pixel, as soon as the bead moves, it may not be possible to retrieve its new coordinates without errors. As the displacement of a bead is computed by the subtraction of the centers of a bead before and after a cell force is applied, the inability to locate exactly this center introduces errors into the recovered displacement. Comparing with the maximum displacement of  $1.9\ \mu\text{m}$  of the problem, the maximum such error is on the order of 5%. This is deemed acceptable. This provides credence of the proposed new algorithm for determining the substrate displacement field.

### 2.7. Application of the present TFM method

We applied the present method to study traction force of human patellar tendon fibroblasts. Briefly, a polyacrylamide gel disk embedded with  $0.2\ \mu\text{m}$  red fluorescent micro-

beads was made. The disk, which was  $120\ \mu\text{m}$  thick and had a diameter of  $10\ \text{mm}$ , was then attached to the bottom of a  $35\ \text{mm}$  glass dish that had a  $14\ \text{mm}$  inner diameter. The gel was a mixture of acrylamide (5%) and bis-acrylamide (0.1%) and red fluorescent polystyrene microbeads of  $0.5\ \mu\text{m}$  in diameter in a density of  $20\ \text{mg beads/ml gel}$ . The Young's modulus of the gel was determined to be  $3\ \text{kPa}$  using the method described in Wang et al (2002).

The gel disk was consecutively pre-treated with  $0.1\ \text{M}$  sodium hydroxide, 3-aminopropyltrimethoxysilane, and  $0.5\%$  glutaraldehyde. The gel surface was then pretreated with Sulfo-Sanpah and coated with  $200\ \mu\text{l}$  of  $100\ \mu\text{g/ml}$  collagen type I overnight. After the cell culture treatment, the confluent cells were trypsinized and placed on collagen-coated polyacrylamide gel disks at  $3000\ \text{cells/disk}$ . The cells were allowed to spread on the gel for 6 hours in the same differentiation medium. Cells with elongated shape on each

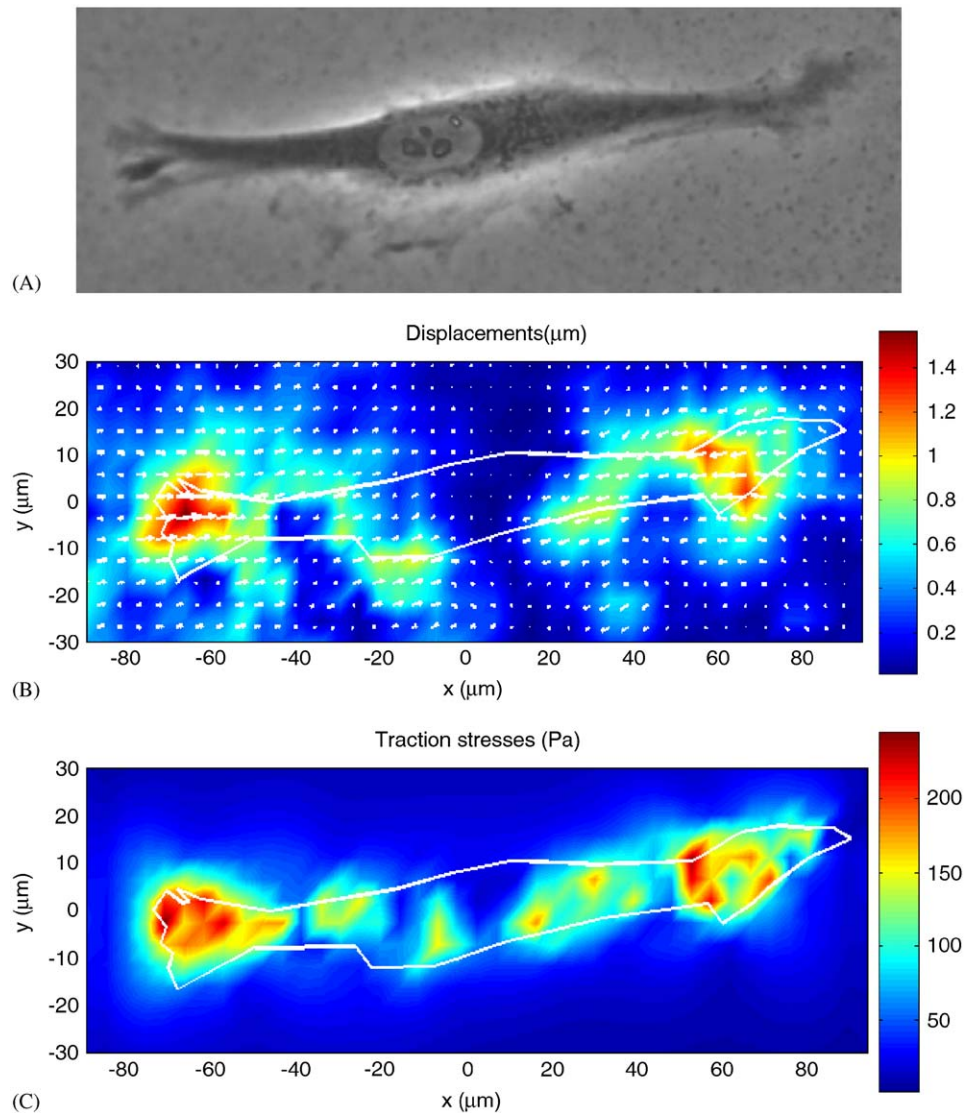


Fig. 6. Application of the present TFM method to human tendon fibroblasts. (A) Human tendon fibroblast on a polyacrylamide gel with embedded fluorescent beads (not shown); (B) substrate displacement field; and (C) cell traction field.

gel were chosen for imaging. First the phase contrast image of the cell and the image of the underneath fluorescent beads were taken. Then, the cells on the gel disk were trypsinized and the image of the fluorescent beads at the same view and the same  $z$  plane was taken. Fig. 6A shows the image of a cell whose traction force is reported herein.

The displacement field and cell traction stress distribution determined by the present method are depicted in Figs. 6B and C. For this particular test sample, the maximum displacement obtained was  $1.2\ \mu\text{m}$ . The cellular forces were concentrated in the front and rear of the cell. This result is consistent with general understanding of traction mechanisms in fibroblasts. The maximum traction stress of 250 Pa found for the fibroblast also appears to be reasonable. These results provide credence to the present method since no *a priori* information has been incorporated.

### 3. Discussion

We have developed a new TFM method to determine cell traction forces. Compared with the existing methods, the present method estimates the displacement field of the substrate based upon the bead movement, and as such, the displacement obtained has a clear meaning. Moreover, the present method solves a forward problem in deriving cell traction force. The 3-D FEM-based algorithms are simple, straightforward, and free from the limitation that a substrate be modeled as an elastic half-space in existing flat substrate TFM methods. A typical force computation takes less than a minute on a single processor 1.2 GHz Pentium 4 personal computer. These characteristics make the present method a viable alternative to the existing TFM methods.

We have presented criteria for matching beads that are displacement magnitude and strain-level dependent. These should not be a problem in practice even for cases without prior experiences on the cells under study. One may start with a set of estimates, and at the end of the analysis, the derived displacement field provides a chance to re-examine the criteria used. Should there be significant discrepancies, a new set of analyses may be conducted using newly obtained values build the identification criteria.

There are several issues that need further research. First, how to quantify the error in the estimated cell traction forces is an important but difficult problem. The use of 3-D FEM no doubt reduces the model error. It is reasonable to infer that the main error comes from the process of estimating the displacement field. This, in turn, may be attributable to the possible mismatch of beads and the errors in pinpointing the bead locations. From our simulation, we concluded that in the process of locating bead centers, there is an intrinsic error, which may contribute an error in displacement equivalent to about 0.42 pixels on the image. The quantification of errors from possible mismatching of beads requires further study. One

possible strategy is to carry out an extensive test program to provide an ensemble of a large suite of data; these data can be used for the evaluation of the consistency of the identification procedure and criteria proposed. In this regard, refinements of some aspects of the laboratory procedure may also be worth pursuing. For instance, could there be an optimal density and an optimal size of beads, respectively, within a gel such that the aforementioned errors can be substantially reduced? Or, could the imaging procedure be improved so that consistent good-quality images can be acquired? Finally, a desirable goal of a TFM would be to track cell traction forces in real time. This would require some adaptive algorithms to be developed to automatically adjust the criteria in the present framework according to the feedback.

### Acknowledgments

This work was supported in part by the NIH Grant AR049921 and the Arthritis Investigator Award from the Arthritis Foundation (JHW). We also gratefully acknowledge anonymous reviewers' thoughtful comments and suggestions.

### References

- Balaban, N.Q., Schwarz, U.S., Riveline, D., Goichberg, P., Tzur, G., Sabanay, I., Mahalu, D., Safran, S., Bershadsky, A., Addadi, L., Geiger, B., 2001. Force and focal adhesion assembly: a close relationship studied using elastic micropatterned substrates. *Nat. Cell Biol.* 3, 466–472.
- Beningo, K.A., Wang, Y.L., 2002. Flexible substrata for the detection of cellular traction forces. *Trends Cell Biol.* 12, 79–84.
- Beningo, K.A., Dembo, M., Wang, Y.L., 2004. Responses of fibroblasts to anchorage of dorsal extracellular matrix receptors. *Proc. Natl. Acad. Sci. USA* 101, 18024–18029.
- Butler, J.P., Tolic-Norrelykke, I.M., Fabry, B., Fredberg, J.J., 2002. Traction fields, moments, and strain energy that cells exert on their surroundings. *Am J Physiol Cell Physiol* 282, C595–C605.
- Dembo, M., Wang, Y.L., 1999. Stresses at the cell-to-substrate interface during locomotion of fibroblasts. *Biophys. J.* 76, 2307–2316.
- Doyle, A.D., Lee, J., 2005. Cyclic changes in keratocyte speed and traction stress arise from  $\text{Ca}^{2+}$ -dependent regulation of cell adhesiveness. *J. Cell. Sci.* 118, 369–379.
- Galbraith, C.G., Sheetz, M.P., 1997. A micromachined device provides a new bend on fibroblast traction forces. *Proc. Natl. Acad. Sci. USA* 94, 9114–9118.
- Galbraith, C.G., Sheetz, M.P., 1998. Forces on adhesive contacts affect cell function. *Curr. Opin. Cell Biol.* 10, 566–571.
- Jacinto, A., Martinez-Arias, A., Martin, P., 2001. Mechanisms of epithelial fusion and repair. *Nat. Cell Biol.* 3, E117–E123.
- Jurado, C., Haserick, J.R., Lee, J., 2005. Slipping or gripping? Fluorescent speckle microscopy in fish keratocytes reveals two different mechanisms for generating a retrograde flow of actin. *Mol. Biol. Cell* 16, 507–518.
- Kiehart, D.P., Galbraith, C.G., Edwards, K.A., Rickoll, W.L., Montague, R.A., 2000. Multiple forces contribute to cell sheet morphogenesis for dorsal closure in *Drosophila*. *J. Cell Biol.* 149, 471–490.
- Landau, L.D., Lifshitz, E.M., 1986. *Theory of Elasticity*, third ed. Pergamon Press, Oxford, UK.
- Lo, C.M., Wang, H.B., Dembo, M., Wang, Y.L., 2000. Cell movement is guided by the rigidity of the substrate. *Biophys. J.* 79, 144–152.

- Marganski, W.A., Dembo, M., Wang, Y.L., 2003. Measurements of cell-generated deformations on flexible substrata using correlation-based optical flow. *Methods Enzymol* 361, 197–211.
- Rajagopalan, P., Marganski, W.A., Brown, X.Q., Wong, J.Y., 2004. Direct comparison of the spread area, contractility, and migration of balb/c 3T3 fibroblasts adhered to fibronectin- and RGD-modified substrata. *Biophys. J.* 87, 2818–2827.
- Tan, J.L., Tien, J., Pirone, D.M., Gray, D.S., Bhadriraju, K., Chen, C.S., 2003. Cells lying on a bed of microneedles: an approach to isolate mechanical force. *PNAS* 100, 1484–1489.
- Wang, N., Tolč-Norrelykke, I.M., Chen, S.J., Mijailovich, S.M., Butler, J.P., Fredberg, J.J., Stamenović, D., 2002. Cell prestress. I. Stiffness and prestress are closely associated in adherent contractile cells. *Am. J. Cell Physiol.* 282, C606–C6156.